The matrix representation of all-fiber gyroscope - numerical calculus and experimental verification

M. SZUSTAKOWSKI, L. R. JAROSZEWICZ
Institute of Technical Physics, Military University of Technology
ul. Kaliskiego 2, 01-489 Warszawa, Poland

A. OSTRZYŻEK
Institute of Electron Technology
Al. Lotników 32/46, 02-668 Warszawa, Poland

1. Introduction

The investigations and development of fiber-optic gyroscopes require the mastering of their theoretical analysis. The fundamental requirement of such an analysis is a simple mathematical description with simultaneous possibility of regarding a variety of partial solutions and preservation of uniform description of the whole device. The Jones calculus fulfilling these requirements is presented in this paper.

A fiber-optic gyroscope is the technical application of a Sagnac interferometer [1]. The optical part of this device, built in a so-called minimum configuration [2] (Fig. 1), allows to determine a rotation rate Ω by measuring the created nonreciprocal phase shift $\Delta\Phi$ between two light beams propagating counter wise. The phase shift $\Delta\Phi$ is detected as a change of light intensity I at the interferometer output [3]:

$$I(\Delta\Phi) = B + A \cdot \cos(\Delta\Phi - \Phi_0), \quad \Delta\Phi = K \cdot \Omega \quad (1a, b)$$

where B is an average intensity level, A is an intensity scale factor, Φ_0 is a phase bias-offset, and K is a constant factor dependent on the sensor loop parameters.

The expression (1a) describes a well-known signal created in the interference system with the main information included in the phase factor. As was shown by J. Sakai [4] for the polarization degree of a fiber and by W. K. Burns [5] for the coherence degree of interfering beams, both parameters for the Sagnac fiber interferometer are kept high being of the order 0.95. Thus, changes of the polarization characteristics influence only the disturbance of the detected signal form (changes in A and Φ_0 values in Eq. 1a).

These characteristics will determine by matrix representations of fiber elements in accordance with the Jones calculus in Sec. 2÷4. Based on that, in Sec. 5 the numerical simulation of gyro operation is described. It allows for the bias-offset and quantum noise level parameters to be calculated. These parameters influence essentially on the sensitivity and the drift, which are the fundamental technical parameters of a fiber gyroscope. The sensitivity is defined as the minimum rotation speed which can be detected by the gyro device; a limit is set by the high frequency noise of the experimental arrangement [6]. The drift, in turn, can be assumed to be the uncertainty of the device in the long term and is strictly tied with low frequency measurement disorders. The above parameters are measured in the built gyro model. Its configuration and results of experimental researches are presented in Sec. 6. The comparison of theoretical and experimental values allows to develop the method of drift limitation.

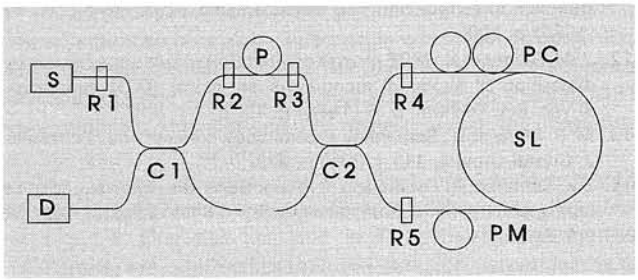

Fig. 1. Minimum configuration of fiber gyroscope; S – source, C1, C2 – couplers, P – polarizer, PC – polarization controller, SL – sensing loop, PM – phase modulator, D – detector, R1, ..., R5 – optical connections

2. Jones calculus

The light wave at any point in the optical system is represented by its Jones vector:

$$\boldsymbol{E} = \begin{bmatrix} E_x \\ E_y \end{bmatrix} \quad (2)$$

The application of that method requires the Jones matrix identification for each sequential element of the optical path. Hence, each of circuit elements is represented by a 2×2 matrix operator applied to the Jones vector $\boldsymbol{E}$. The operation of the whole optical system can be described by the product of these matrices, according to the rules of Jones calculus [7].

The Jones calculus is limited only to a monochromatic, fully polarized wave. However, as was shown in [8], the light source description by means of the coherence matrix:

$$\boldsymbol{J} = \begin{bmatrix} \langle E_x E_x^* \rangle & \langle E_x E_y^* \rangle \\ \langle E_y E_x^* \rangle & \langle E_y E_y^* \rangle \end{bmatrix} \quad (3)$$

where $\langle \ldots \rangle$ is an average over observation time and * means the coupling operation of a proper component of the field E, allows to consider additionally a partial polarization of the source. In such case, the coherence matrix of the output beam $\boldsymbol{J}_{wy}$ is used as the characteristic parameter which depends on the source coherence matrix $\boldsymbol{J}_z$ as well as on the Jones matrix of the described system $\boldsymbol{M}$ [8]:

$$\boldsymbol{J}_{wy} = \boldsymbol{M} \cdot \boldsymbol{J}_z \cdot \boldsymbol{M}^+ \quad (4)$$

$\boldsymbol{M}^+$ is a matrix Hermitian conjugate with matrix $\boldsymbol{M}$. If the coherence matrix on the output of optical system is known then the output light can be determined as

$$I = \mathrm{Tr}(\boldsymbol{J}_{wy}) \quad (5)$$

where $\mathrm{Tr}\boldsymbol{J}$ is a trace of the matrix $\boldsymbol{J}$.

In classical optics the above formalism is well known. The matrix representation of such elements as: isotropic and anisotropic optical paths, polarizers polarization controllers, optical modulators, etc. are determined in Ref. [9]. Application of the Jones calculus to the all-fiber gyroscope requires the creation of its matrix representation analogous as in classical optics. The foundations of introducing such a representation for single-mode fibers, with assumption of the quasi-monochromatic light source are presented below.

3. Matrix representation of a single-mode optical fiber

An ideal single-mode optical fiber is an isotropic waveguide medium carrying two degenerate polarization eigenstates $\vec{e}_1, \vec{e}_2$ [10]. They have the same spatial field distributions, propagation constants $\beta_1 = \beta_2 = \beta_3$ and linear, perpendicular each to other polarization states. Assuming two eigenstates as the basis vectors

$$\boldsymbol{E}(z) = E_x \cdot \vec{e}_1 + E_y \cdot \vec{e}_2 = \begin{bmatrix} E_x \\ E_y \end{bmatrix} \tag{6}$$

leads, in the Jones calculus, to the determination of an ideal single-mode fiber by means of the matrix

$$\boldsymbol{M} = \mathrm{e}^{-\mathrm{j}\beta z}\begin{bmatrix} 1 & 0 \\ 0 & 1 \end{bmatrix} \equiv \boldsymbol{D}(\beta z) \tag{7}$$

In this case an optical fiber is equivalent physically to the constant phase delayer (matrix $\boldsymbol{D}$) with the delay of βz, so it does not change the polarization of light wave.

The polarization eigenstates and propagation constants (β_1, β_2) can be changed by elasto-optic deformation, and the fiber becomes an anisotropic medium with a determined value of birefringence $\Delta\beta = |\beta_1 - \beta_2|$ [11]. The changes introduced by deformation are determined by a modified coupled modes theory. As it was shown by J. Sakai [12], a single elastic deformation homogeneous along the fiber of length z is described by the following Jones matrix:

$$\boldsymbol{M} = \exp\left[-\mathrm{j}\frac{N_{11} + N_{22}}{2} \cdot z\right]\begin{bmatrix} m_1 & -m_2^* \\ m_2 & m_1^* \end{bmatrix} \tag{8a}$$

where

$$m_1 = \cos\left(\frac{\Delta\beta z}{2}\right) - \mathrm{j} \cdot \left[\frac{N_{11} - N_{22}}{\Delta\beta}\right] \cdot \sin\left(\frac{\Delta\beta z}{2}\right); \tag{8b}$$

$$m_2 = -\mathrm{j} \cdot \left(\frac{2N_{21}}{\Delta\beta}\right) \cdot \sin\left(\frac{\Delta\beta z}{2}\right) \tag{8c}$$

while birefringence forced by the deformation is expressed as

$$\Delta\beta = |\beta_1 - \beta_2| = [(N_{11} - N_{22})^2 + |2N_{12}|^2]^{1/2} \tag{9a}$$

where

$$N_{ll} = \beta + \omega \cdot \varepsilon_0 \int \vec{e}_l^{\,*}[\delta\varepsilon]\vec{e}_l \, ds \;\; (l = 1, 2),$$
$$N_{lm} = N_{ml}^* = \omega \cdot \varepsilon_0 \int \vec{e}_l^{\,*}[\delta\varepsilon]\vec{e}_m \, ds \;\; (l \neq m) \tag{9b}$$

Integration is carried out over the fiber cross-section, * means the conjugate operation, β is the propagation constant of the non-disturbed system, ε_0 is the vacuum permittivity, ω is the angular frequency of radiation and $[\delta\varepsilon]$ is the disturbance tensor equivalent to elastic deformation.

Similar solutions are obtained when the fiber is actuated by the set of m-th order elastic deformation with different intensities and directions (Fig. 2). The analysis of Eqs. (8÷9) shows that changes of polarization in the fiber are described by $2N_{21}$, $(N_{11} - N_{22})$ and not by individual expressions N_{lm}, so for multiply disturbed optical fiber, these parameters, as was shown in [13], are the following:

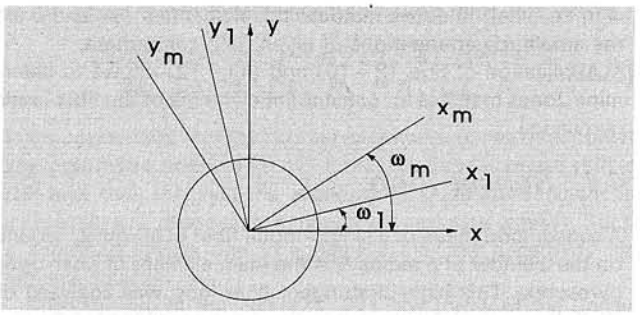

Fig. 2. The fiber cross-section and direction of m-th order disturbance action. The propagation direction z was assumed

$$(N_{11} - N_{22}) = \sum_m \Delta\beta_m \cdot \cos(2\omega_m), \tag{10a}$$

$$2N_{21} = \sum_m \Delta\beta_m \cdot \sin(2\omega_m) + \sum_m 2N_{21,m}^{(0)} \tag{10b}$$

Here, $\Delta\beta_m$ is a birefringence caused by m-th order disturbance with main axes directed along the x, y axes. The factor $N_{21,m}^{(0)}$ is a coupling coefficient of $N_{21}^{(0)}$ for the disturbance m, being the result of the deformation described by a tensor with off-diagonal elements. The above equations contain the sum of each component of birefringence $\Delta\beta_m$ projected on the x,y axes, except for the expression for the rotation of the optical polarization ($2N_{21,m}^{(0)}$). The projecting angle is two times greater than the angle ω_m between the disturbance axis and the assumed laboratory system (Fig. 2). Thus, by means of Eqs. (8÷10), it is possible to determine the Jones matrix for a fiber creating a given optical element.

4. Matrix representation of all-fiber gyroscope elements

According to the theorem of equivalence of Jones and Hurwitz optical systems [14], it is possible for each fiber element to create its functional operation scheme of the form:

$$\boldsymbol{M} = \prod_{j,k,l} \boldsymbol{P}_j \cdot \boldsymbol{R}_k \cdot \boldsymbol{G}_l \tag{11}$$

where the matrices ***P, R, G*** represent fundamental optical elements as:

1. ***R*** — matrix of the polarization rotating elements (rotator) of form:

$$\boldsymbol{R}(\theta) \equiv \begin{bmatrix} \cos\theta & -\sin\theta \\ \sin\theta & \cos\theta \end{bmatrix}, \tag{12a}$$

where θ is the rotation angle of polarization during light transmission through this element.

2. ***G*** — matrix of a linear phase retarder (Eq. 12b):

$$\boldsymbol{G}(\delta) \equiv \begin{bmatrix} \mathrm{e}^{\mathrm{j}\delta} & 0 \\ 0 & \mathrm{e}^{-\mathrm{j}\delta} \end{bmatrix}, \quad \boldsymbol{D}(\Delta) \equiv \mathrm{e}^{-\mathrm{j}\Delta} \cdot \begin{bmatrix} 1 & 0 \\ 0 & 1 \end{bmatrix} \tag{12b, c}$$

where 2δ is a measure of birefringence introduced by this element. The matrix of constant phase delayer (matrix $\boldsymbol{D}$ in Eq. 12c) is the particular case of that one, where Δ is a phase delay of light wave during transmission through the given optical element.

3. ***P*** — matrix of a polarizer (Eq. 12d):

$$\boldsymbol{P}(p_1, p_2) \equiv \begin{bmatrix} p_1 & 0 \\ 0 & p_2 \end{bmatrix}, \; \boldsymbol{A}(p) \equiv \begin{bmatrix} p & 0 \\ 0 & p \end{bmatrix}, \; p < 1 \tag{12d, e}$$

the particular case of which is the matrix of an absorber (matrix

$\boldsymbol{A}$ in Eq. 12e). In above matrices the elements p_1, p_2 and p are the amplitude attenuations of given field component.

Application of Eqs. (8÷10) and (11÷12) allows to determine Jones matrices for constituent elements of the fiber-optic gyroscope.

4.1. Sensor loop

A sensor loop made of a single-mode fiber of length L, wound on the cylinder of a radius R is the main element of fiber-optic gyroscope. This high-birefringent fiber loop was analyzed by W. K. Burns [15]. Using that analysis it is possible to show that the Jones matrix for a fiber of length L, birefringence $\Delta\beta$ and bandwidth of light source $\delta\omega$ has the form [3]:

$$\boldsymbol{F}(L, \Delta\beta, \delta\omega) = \boldsymbol{D}(\beta L) \cdot \boldsymbol{G}(\delta_2) \cdot \boldsymbol{R}(\omega) \cdot \boldsymbol{G}(\delta) \cdot \boldsymbol{R}(\omega) \cdot \boldsymbol{G}(\delta_1) \tag{13}$$

where

$$\delta_1 = \Delta\beta L_\gamma/4 - \varphi_1, \quad \delta_2 = \Delta\beta L_\gamma/4 + \varphi_2,$$

$$\delta = \Delta\beta(L - L_\gamma)/2 + (\varphi_1 - \varphi_2), \quad \omega = -\sqrt{hL_\gamma},$$

and characteristic parameters for a high-birefringent fiber: depolarization length – L_γ, crosstalk – h, and phase disturbances – φ_1, φ_2 related with mode coupling for both fiber ends.

For a high-birefringent fiber $L_\gamma \approx 16.5$ cm and $h = 1.6 \cdot 10^{-5}\ \mathrm{m}^{-1}$ [15] and it can be shown from Eq. (13) that $\omega \approx 1.63 \cdot 10^{-3}$ rad. The rotation matrices $\boldsymbol{R}(\omega)$ appear as unit ones, which means no rotation. As can be seen, the sensor loop is equivalent to the phase retarder with precisely defined axes, which can be written as:

$$\boldsymbol{F}(L, \Delta\beta, \delta\omega) = \boldsymbol{D}(\beta L) \cdot \boldsymbol{G}(\Delta\beta L/2) \tag{14}$$

4.3. Phase modulator

A phase modulator, placed at one end of the sensor loop, allows a maximum sensitivity to be achieved for a small rotation speed. In the fiber version it is built as a certain number of fiber turns wound in one layer on a cylinder piezoceramic. Assuming that the wound fiber has a certain core ellipticity e, and a twist of the rate Φ_t, its winding into an N-turn loop of radius R causes the induced birefringence. This birefringence gives a matrix characteristic of the modulator, which, by means of eqs.(8÷12), can be expressed as [3]:

$$\boldsymbol{M}(N, e, R, \Phi_t) \equiv \boldsymbol{D}(\beta' L) \cdot \boldsymbol{R}(\theta) \cdot \boldsymbol{R}(\Phi_t L) \cdot$$

$$\cdot \boldsymbol{R}(\omega_t) \cdot \boldsymbol{R}(-\omega_t) \cdot \boldsymbol{G}(\rho) \cdot \boldsymbol{R}(\omega_t)\, \boldsymbol{R}(\omega_t) \cdot \boldsymbol{R}(-\theta), \tag{15}$$

where

$$\omega_t = -0.5 \tan^{-1}\left[\frac{\Phi_t - K_t}{Z} \tan(ZL)\right],$$

$$\omega_t = -0.5 \tan^{-1}\left[\frac{K_R \sin(2\theta)}{K_e + K_R \cos(2\theta)}\right]$$

$$\rho = \tan^{-1}\left(\frac{\cos(2\omega_t)}{\cos(2\omega_1)} \cdot \frac{K_e + K_R \cos(2\theta)}{Z} \tan(ZL)\right], \quad L = 2\pi RN$$

and

$$Z = [K_e^2 + K_R^2 + 2K_e K_R \cos(2\theta) + (\Phi_t - K_t)^2]^{1/2} \tag{16}$$

It was assumed that at the initial point of winding the ellipticity axis of the fiber core makes the angle θ (Fig. 3) with the surface f piezoceramic tube. Values $2K_e$, $2K_R$ and $2K_t$ are temporary birefringences induced by individual deformations of core ellipticity, fiber bend and fiber twist respectively.

The analyzed phase modulator, besides the birefringence 2ρ, introduces additionally the rotation of the polarization state of the angle $(-2\omega_1 + \Phi_t L)$, in relation to the phase retarder axis on the modulator input.

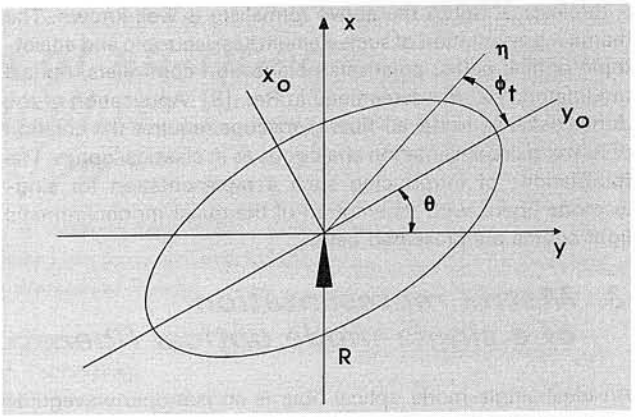

Fig. 3. The system of axes adopted for the phase modulator description

4.4. Polarization controller

The modulator and sensor loop birefringence can lead to changes of polarization state of the interfering light beams. In order to fit the polarization state of both beams, a system of polarization controller is placed at one of the ends of the sensor loop. This element can be made on the basis of quarterwave Lefever loops [16]. The matrix analysis of the polarization controller activity described in paper [17] gives its matrix characteristic as:

$$\boldsymbol{CP}(\psi, \varphi) = \boldsymbol{D}(\beta L) \cdot \boldsymbol{R}(\omega_\psi) \cdot \boldsymbol{G}(\delta) \cdot \boldsymbol{R}(-\omega_\varphi) \tag{17}$$

where $\omega_\psi = g\psi - \pi/4$, $\omega_\varphi = g\varphi + \pi/4$, $\delta = \pi/2 + (\varphi - \psi)$ $g = 0.92$ and φ, ψ are setting angles of quarter-wave loops.

As can be observed, the rotation of fiber loops causes the changes of rotation angle (in a rotator matrix $\boldsymbol{R}$) and birefringence (in a phase retarder matrix $\boldsymbol{G}$). These changes cause a change of light polarization state (azimuth and ellipticity), which allows for optional compensation of polarization changes.

4.5. Fiber coupler

A fiber coupler allowing on interfering assembly of both beams was described using Jones calculus by L. Chen [18]. For an ideal coupler of length L, made of the fiber with birefringence $\Delta\beta$, the Jones matrices of the beam passing through the coupler ($\boldsymbol{CT}$) and reflected one ($\boldsymbol{CR}$) are as follows [18]:

$$\boldsymbol{CT}(L, \Delta\beta, K) = \boldsymbol{D}(\beta L) \cdot \boldsymbol{A}(\cos KL) \cdot \boldsymbol{G}(-\Delta\beta L/2) \tag{18a}$$

$$\boldsymbol{CR}(L, \Delta\beta, K) = \boldsymbol{D}(\beta L) \cdot \boldsymbol{D}(\pi/2) \cdot \boldsymbol{A}(\sin KL) \cdot \boldsymbol{G}(-\Delta\beta L/2) \tag{18b}$$

where K is a interfiber coupling coefficient. For such a coupler the output polarization state is identical with the polarization state at the output of the fiber with the same birefringence and length as the coupler. However, the equality of power distributions between the branches requires the fulfillment of the condition that $KL = \pi/4 + 2n\pi$.

4.6. Polarizer

As was shown by Kinter [19] for the operation of the fiber-optic gyroscope, the polarizer extinction ratio ε has a practical importance. Writing the polarizer as a linear polarization filter with negligible transmission losses leads to the matrix characteristic of this element of the form [3]:

$$\boldsymbol{P}(\varepsilon) = \begin{bmatrix} 1 & 0 \\ 0 & \varepsilon \end{bmatrix} \equiv \boldsymbol{P}(1, \varepsilon) \tag{19}$$

4.7. Light source

Assuming the approximation of quasi-monochromaticity, the light source of the polarization degree P radiating an elliptically polarized wave of azimuth v and ellipticity e, is defined by a coherence matrix of the type [8]:

$$\boldsymbol{J}_z = \frac{1}{2}\cdot\begin{bmatrix} 1 - P\cos 2v\cos 2e & P(\sin 2v\cos 2e - j\sin 2e \\ P(\sin 2v\cos 2e + j\sin 2e) & 1 + P\cos 2v\cos 2e \end{bmatrix} \tag{20}$$

5. Simulation of all-fiber gyroscope

Fig. 4 shows an equivalent lumped element representation (ELER) of all-fiber gyroscope built with optical devices according to Fig. 1. The devices in the Fig. 4 are the Jones matrices described in Sec. 4 for polarizer $\boldsymbol{P}$, phase modulator $\boldsymbol{M}$, polarization controller $\boldsymbol{CP}$, sensing loop $\boldsymbol{F}$ and reflective $\boldsymbol{CR}$ and transmissive $\boldsymbol{CT}$ ways of the coupler. Rotation matrices $\boldsymbol{R}_1,\ldots,\boldsymbol{R}_5$ represent a misalignment of birefringence axes between elements. An additionally introduced inversion matrix $\boldsymbol{Inv}$ determines a reflection of the system axes occurring at the pass light through the sensor loop.

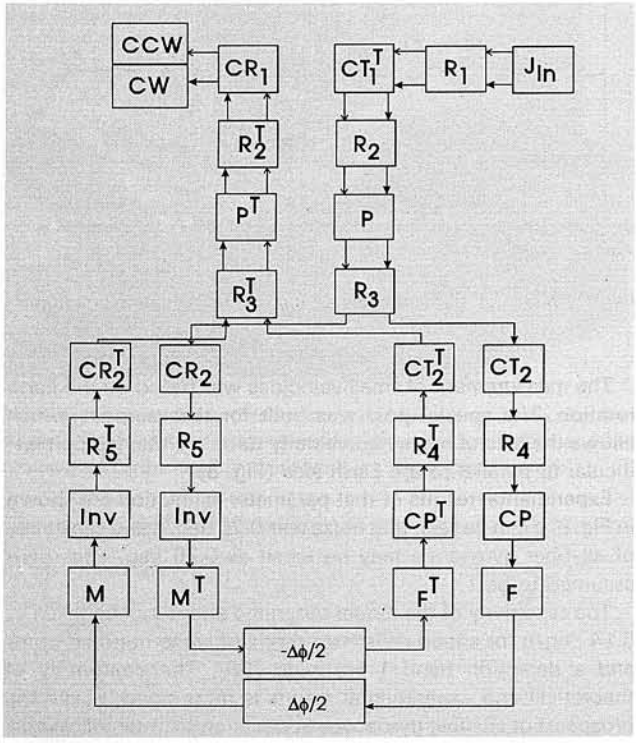

Fig. 4. Equivalent lumped element representation (ELER) of all-fiber gyroscope; ⟶ cw direction, ⇢ ccw direction

Assuming that the Sagnac effect is the only nonreciprocal effect in the fiber-optic gyroscope, the wave passing through a given element in the opposite direction is described by the transposed Jones matrix. Knowledge of matrices of the gyroscope devices allows one to write the Jones matrix for the whole gyro in the following form [3]:

$$\boldsymbol{Z} = \boldsymbol{CW}\cdot e^{j\Delta\Phi/2} + \boldsymbol{CCW}\cdot e^{j(\pi/2-\Delta\Phi/2} \tag{21}$$

where

$$\boldsymbol{CW} = \boldsymbol{CR}_1^T\cdot\boldsymbol{R}_2^T\cdot\boldsymbol{P}^T\cdot\boldsymbol{R}_3^T\cdot\boldsymbol{CR}_2^T\cdot\boldsymbol{R}_5^T\cdot\boldsymbol{Inv}\cdot\boldsymbol{M}\cdot\boldsymbol{F}\cdot \boldsymbol{CP}\cdot\boldsymbol{R}_4\cdot\boldsymbol{CT}_2\cdot\boldsymbol{R}_3\cdot\boldsymbol{P}\cdot\boldsymbol{R}_2\cdot\boldsymbol{CT}_1\cdot\boldsymbol{R}_1 \tag{22a}$$

is the Jones matrix for the clockwise (cw) direction, while

$$\boldsymbol{CCW} = \boldsymbol{CR}_1^T\cdot\boldsymbol{R}_2^T\cdot\boldsymbol{P}^T\cdot\boldsymbol{R}_3^T\cdot\boldsymbol{CT}_2^T\cdot\boldsymbol{R}_4^T\cdot\boldsymbol{CP}^T\cdot\boldsymbol{F}^T\cdot \boldsymbol{M}^T\cdot\boldsymbol{Inv}\cdot\boldsymbol{R}_5\cdot\boldsymbol{CR}_2\cdot\boldsymbol{R}_3\cdot\boldsymbol{P}\cdot\boldsymbol{R}_2\cdot\boldsymbol{CT}_1\cdot\boldsymbol{R}_1 \tag{22b}$$

is the Jones matrix for the counter-clockwise (ccw) direction. It was assumed a priori, in Eq. (21), that the Sagnac phase shift is $\Delta\Phi$ and that the systems working in quadrature (there is a constant $\pi/2$ phase shift between cw and ccw waves). Such a condition allows one to achieve a maximal sensitivity for minimal rotation rate.

Substituting, in the Eqs. (21, 22), the forms of the Jones matrix for individual devices defined in Sec. 4 allows, through relations (4, 5), a numerical simulation of the gyroscope operation. The output signal achieved in this case, compatible with the relation (1), depends on a group of 36 parameters characterizing fiber devices. The influence of these parameters on the form of detected signal (values A and Φ_0 in Eq. 1a) can be numerically calculated [3].

Fig. 5 presents the results of a simulation of all-fiber gyroscope performance. The misalignments of birefringence axes in connections of the coupler with polarizer (matrix $\boldsymbol{R}_2$), and coupler with sensor loop end (matrix $\boldsymbol{R}_5$) were assumed to be variable parameters. Physically it seems that the state of polarization (SOP) of the beam input at the polarizer and the beam input from one end of the coupler to the high-birefringent fiber of the sensor loop are mismatched.

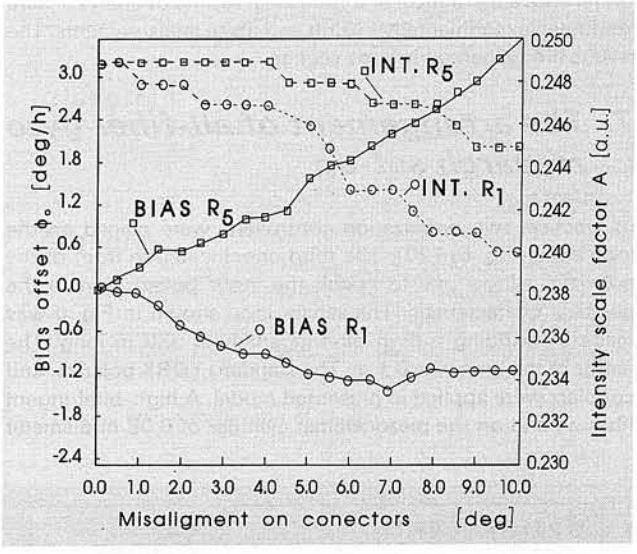

Fig. 5. Changes of intensity scale factor (A) and phase bias-offset (Φ_0) versus angle of the misalignment of element birefringence axis (matrices $\boldsymbol{R}_2$ and $\boldsymbol{R}_5$)

As may be noticed, the wave SOP change before the polarizer causes changes of intensity scale factor mainly, and this in turn influences the systems sensitivity. The axis misalignment between coupler and sensor loop end generates a great bias-offset value which is shown as the system drift.

The general analysis of drift in Ref. [20] shows that the main components of drift are the fiber birefringence changes. A phase bias-offset which is source of it can be expressed as:

$$\Delta\Phi_0 \approx \frac{\mathrm{Im}\left(\varepsilon(p_{11}p_{21}^* - p_{11}^*p_{12})xy^* + \varepsilon^2 p_{12}p_{21}(|y|^2 - |x|^2)\right)}{|p_{11}x|^2 + \varepsilon^2|p_{22}y|^2} \tag{23}$$

where ε — polarizer extinction ratio, p_{11}, p_{21} and p_{12} — Jones components describing loop fiber, x, y — components of source polarization vector (as the Jones vector $x = E_x$, $y = E_y$).

An extinction ratio appears as the main part of the phase error and it depends on a polarization modes relation which is expressed by a $x \cdot y^*$ factor. The slow phase changes between x and y are the drift components because they exist in a detected band in the 1 Hz range. The quick phase changes will cause the shift of considered drift component beyond the detection band what is possible by source power modulation. The changes of phase relations between the TE and TM modes of a semiconductor laser can be induced by variations of supply current [21]. Than, the average frequency of emitted light is changed too, what is profitable effect because the Sagnac phase measurement error is the result of inequality of optical distances. At the same time the frequency change causes the phase shift variation and if the speed of these changes is suitable they will be removed beyond the band of detection. The modulation does not induce disorders in the detected signal.

The next part of the error expressed by equation (23) depends on ε^2 and can be limited by the equalization of the polarization modes in front of the polarizer, $|x| = |y|$. The same effect can be obtained by the introduction of phase changes between components p_{12} and p_{21} and frequencies chosen beyond the detection band.

The gyro sensitivity particularly depends on quantum and thermal noise as was shown in [20]. For that reason, the possibly high value of photodiode load resistance appears as a substantial component of sensitivity increase.

The above theoretical and numerical results of analysis were confirmed experimentally by drift and noise measurements. The results are presented in next section.

7. The arrangement of all-fiber gyro research set-up

In practice, two polarization controllers, were placed on the loop ends (Fig. 6) [20]. The third one, located in front of the polarizer, allows one to match the input polarization to the polarizer characteristic. The sensor loop shown in Fig. 6 was made by winding a high-birefringent fiber 380 m long. The radius of the loop was 0.1 m. The standard YORK polarizer and couplers were applied in presented model. A high-birefringent fiber wound on the piezoceramic cylinder of 0.08 m diameter

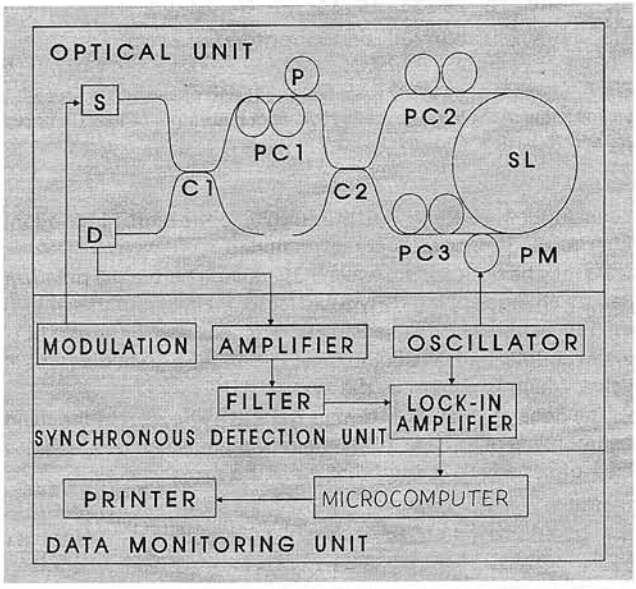

Fig. 6. The arrangement of Sagnac fiber interferometer model: S – laser, D – detector, C1, C2 – couplers, PC1, ..., PC3 controllers, P – polarizer, PM – phase modulator, SL – sensor loop

was applied as a phase modulator used for synchronic detection. The required $\pi/2$ phase shift was obtained for 144 kHz and 0.85 V.

The connections between elements were made by fusion. The total loss was estimated as 26 dB. The source of light, a semiconductor GaInAsP laser, has an output power for $\lambda = 1.3$ μm in the 1 mW range. The detected signal passing a low noise amplifier had been synchronically processed and then the results were displayed on the monitor screen (Fig. 6).

The registration of Sagnac phase shift caused by the rotation, the noise and drift estimation was possible by suitable microcomputer processing (Fig. 7) [20]:

$$\text{Drift} = \frac{K}{(t_2 - t_1)} \int_{t_1}^{t_2} v(t)\,dt,$$
$$\text{Noise} = \left[\frac{K}{(t_2 - t_1)} \int_{t_1}^{t_2} \left(v(t) - \frac{\text{Drift}}{K} \right)^2 dt \right]^{1/2} \quad (24)$$

where t_1, t_2 – the initial and final time of drift and noise estimation, K – scale factor dependent on measured signals amplification, $v(t)$ – registered results related to rotation velocity.

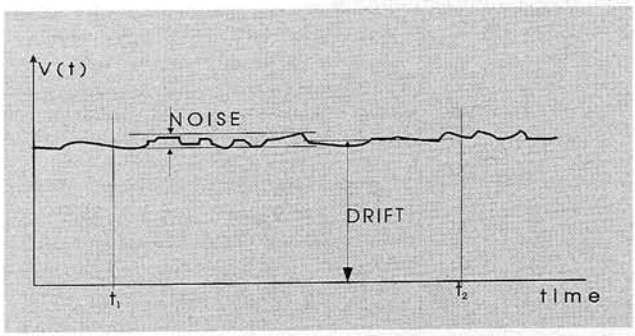

Fig. 7. An idea of drift and noise estimation. Non-rotating conditions

The measurement of small velocities was based on the Earth rotation. The special post was built for that purpose which allows the axis of measured velocity to be maintained perpendicular or parallel to the Earth axis (Fig. 8).

Experimental results of that parameter estimation are shown in Fig. 9. It can be seen that noise was 0.25 deg/h and sensitivity of all-fiber gyroscope may be taken as 0.25 deg/h for SNR assumed to be 1.

The sensitivity of the model described above can be taken as 0.14 deg/h for a load resistance range of some hundred ohms and a detection band 1 Hz wide [20]. The conformity of theoretical and experimental results is quite good, hence the prospects of all-fiber gyroscope application for internal navigation systems appear reasonable.

The correctness of the model was tested on the basis of Earth rotation measurements (Fig. 10). For that purpose the axis sensor loop was positioned according to cardinal points. It can be noticed that the value and rotation direction are recorded correctly. The lack of zero points in the W–E setting was caused by adjustment troubles.

The long term recording results are shown in Fig. 11. The system was set in the W–E direction, which allows one to measure the drift only (rotation is eliminated). It is easily noticed that drift was about 5 deg/h.

The theoretical analysis presented in Sec. 6 was shown so drift may be limited by the source modulation, than the laser power was modulated by 100% fulfilled rectangular signal. The results are shown in Fig. 12.

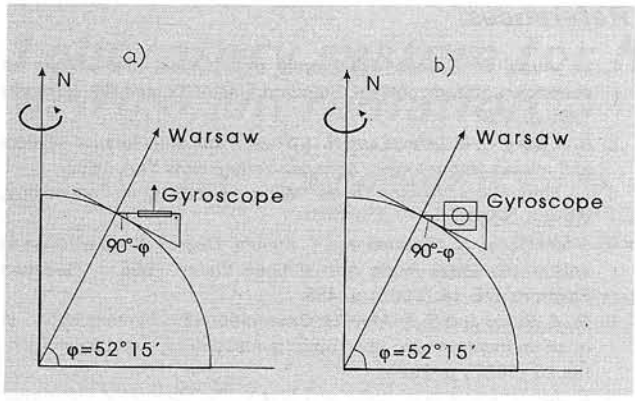

Fig. 8. An arrangement for Earth rotation measurements: a) the axes are parallel (Earth rotation measurements), b) axes perpendicular (the influence of Earths rotation eliminated), c) interferometer model

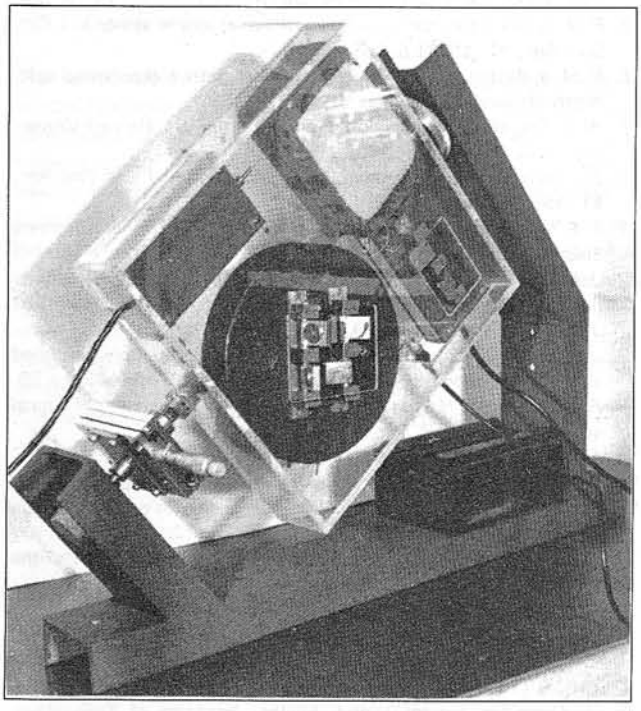

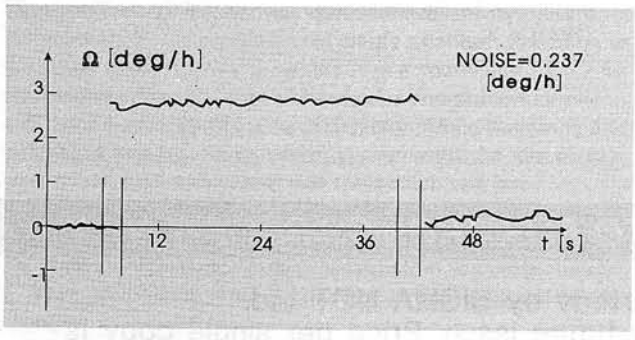

Fig. 9. Sensitivity of interferometer (experimental results)

The light source modulation allowed the system drift to be reduced by a factor of about four to 1.25 deg/h. A suitable matching of modulation amplitude may be the way to achieve farther drift limitation. For that purpose it is necessary to know the dynamic properties of the semiconductor laser. The modulation of phase components between birefringence modes appears as technically easier. It is possible for the system to be made completely with high-birefringent fiber.

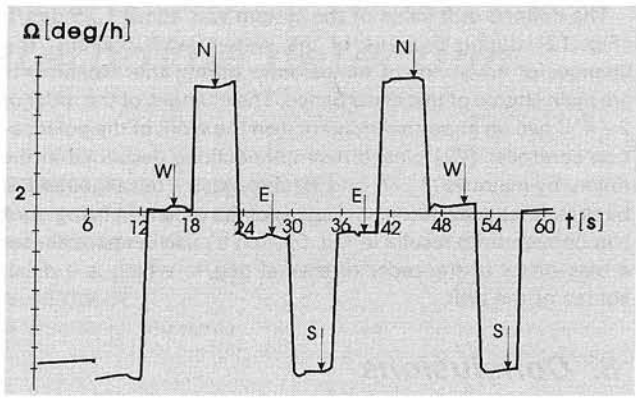

Fig. 10. Registration of rotation speed according to the system setting in relation of the globe

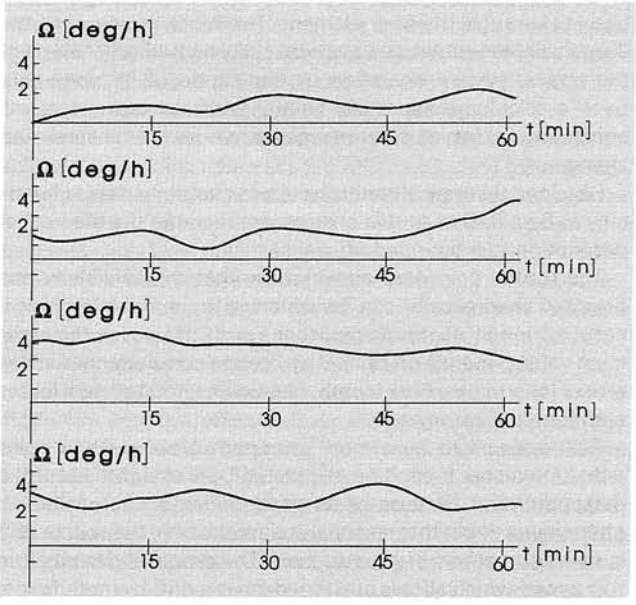

Fig. 11. Long term stability-drift of system

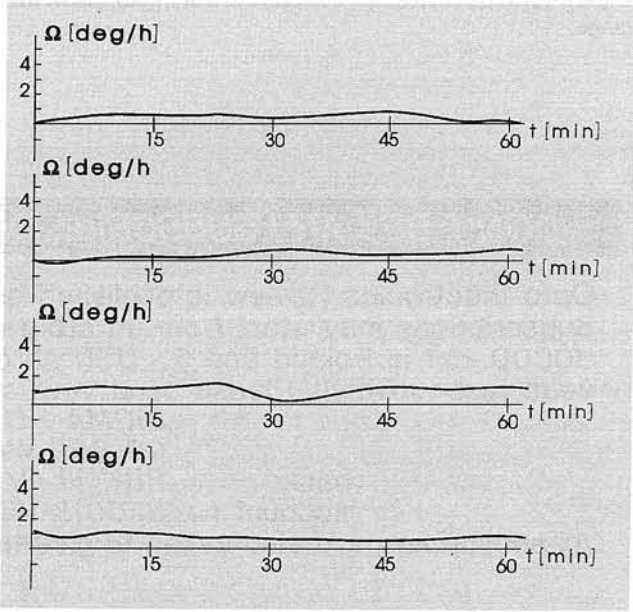

Fig. 12. Drift of the system in the case of light source power modulation

The defined drift value of the system was about 1.25 deg/h (Fig. 12) during 5 hours of the system was working. The changes of environment temperature during the experiments are main source of this disturbance. The changes of the order of $2 \div 4°C$ had an important influence on the work of the polarization controller [22] placed near connections described in the theory by matrices $\boldsymbol{R}_2$, $\boldsymbol{R}_5$ and $\boldsymbol{R}_4$. It caused a misalignment of birefringence axes between devices of the order of 10 deg. As it can be seen from results in Fig. 5, such a misalignment causes a bias-offset of the order of several deg/h, which is a direct source of the drift.

8. Conclusions

The achieved results show that the Jones calculus can be used for the description of fiber elements. With the application of Jones calculus, it is possible to analysis the influence of device parameters on the changes of the polarization of a light beam passing through the fiber element. The block structure of the Jones calculus allows an easy, especially numerical, analysis of the optical system operation by simulation of its operation. Such a calculus is especially helpful while analyzing systems containing a lot of fiber elements whose parameters can change.

Obtained theoretical results have been confirmed experimentally in Sec. 6. Due to this one can assume that the theoretical description is proper and efficient.

The results presented above show that the sensitivity anticipated theoretically can be obtained by suitable technical construction of electronic gyroscope parts. However, the minimum value depends on optical gyroscope components such as sensor loop radius, fiber length, fiber losses, total system losses and light source power.

Drift appears to be a more important problem than noise reduction alone. It can't be eliminated by a straightness of the detection band because of its dependence on nonreciprocal phenomena. From that reason the elimination of the source drift is the best method of its reduction. The proposal described in this paper, which allows one to reduce the drift by modulation, may be a good way, nevertheless it is only a half-measure.

Application of all-fiber gyroscope as an inertial navigation system requires sensitivity of 0.01 deg/h range, while drift has to be less than 0.5 deg/h. Our experimentally obtained results show that the parameters are one order of magnitude below this range.

References

1. *W. Auch, D. Rashlfs:* Fiber optic gyro system applications on strapdown attitude control. Standard Electric Lorenz AG, Stuttgart 1985, p. 3.0.
2. *R. A. Berg, H. C. Lefevre and H. J. Shaw:* Fiber optic rotation sensors and related technologies. Springer-Verlag, New York 1982.
3. *L. Jaroszewicz:* Doctor Thesis. Military Academy of Technology, Warsaw 1988.
4. *J-Ichi Sakai, S. Machida* and *T. Kimura:* Degree of polarization in anisotropic single-mode optical fiber: theory. IEEE J. Quantum Electron., **QE-18** (1982) p. 488.
5. *W. K. Burns* and *R. P. Moeller:* Observation of coherence effects in quasi-monochromatic fiber-optic gyroscope. J. Lightwave Technol., **5** (1987) p. 1024.
6. *E. Jones:* Analysis of noise and bias in the fiber optic gyroscope. Proc. 1st Int. Conf. Opt. Fiber Sensor OFS83, London 1983, p. 138.
7. *R. G. Jones:* A new calculus for treatment of optical systems. J. Opt. Soc. Am., **31** (1941) p. 488.
8. *R. M. A. Azzam* and *N. M. Bashena:* Ellipsometry and polarized light. North-Holland, Amsterdam 1977.
9. *W. A. Shurkliff:* Polarized light production and use. Harvard University Press, Cambridge 1962.
10. *E. Snitzer:* Cylindrical dielectric waveguide modes. J. Opt. Soc. Am., **51** (1961) p. 491.
11. *I. P. Kaminow:* Polarization in optical fiber. IEEE J. Quantum Electron. **QE-17** (1981) p.15.
12. *J. I. Sakai* and *T. Kimura:* Birefringence and polarization characteristics of single mode optical fiber under elastic deformations. IEEE J. Quantum Electron., **QE-17** (1981) p. 1041.
13. *J. I. Sakai, T. Kimura:* Polarization behavior in multiply perturbed single-mode fibers. IEEE J. Quantum Electron., **QE-18** (1982) p. 59.
14. *R. G. Jones* and *H. Hurwitz:* A new calculus for treatment of optical systems. J. Opt. Soc. Am., **31** (1941) p. 493.
15. *W. K. Burns:* Phase error bounds of fiber gyro with polarization-holding fiber. J. Lightwave Technol., **4** (1986) p. 8.
16. *H. C. Lefevre:* Single-mode fractional wave devices and polarization controllers. Electron. Lett., **16** (1980) p. 778.
17. *M. Szustakowski* and *L. Jaroszewicz:* The matrix analysis of the polarization transformer. MAT report., **435** (1988) p. 3.
18. *C-L. Chen, W. K. Burns:* Polarization characteristics of single-mode couplers. IEEE J. Quantum Electron., **QE-18** (1982) p. 1589.
19. *E. C. Kinter:* Polarization control in optical fiber gyroscopes. Opt. Lett., **6** (1981) p. 154.
20. *A. Ostrzyżek:* Doctor Thesis. Military Academy of Technology, Warsaw 1989.
21. *A. Dandridge:* Fiber optic rotation sensors and related technologies. Springer-Verlag, New York 1982.
22. *M. Szustakowski, L. Jaroszewicz:* The change of the state of polarization by the single mode fiber (in Polish). Elektronika, **27** (1987) p. 3.